21FFL-0201

The effect of spark-plug heat dispersal range and exhaust valve opening timing on cold-start emissions and cycle-to-cycle variability

Author, co-author (Do NOT enter this information. It will be pulled from participant tab in MyTechZone)
Affiliation (Do NOT enter this information. It will be pulled from participant tab in MyTechZone)

Abstract

The partnership for advancing combustion engines (PACE) is a US Department of Energy consortium involving multiple national laboratories and includes a goal of addressing key efficiency and emission barriers in light-duty engines fueled with a market-representative E10 gasoline. A major pillar of the initiative is the generation of detailed experimental data and modeling capabilities to understand and predict cold-start behavior. Cold-start, as defined by the time between first engine crank and three-way catalyst light-off, is responsible for a large percentage of NOx, unburned hydrocarbon and particulate matter emissions in light-duty engines. Minimizing emissions during cold-start is a trade-off between achieving faster light-off of the three-way catalyst and engine out emissions during that period. In this study, gaseous and soot emissions were measured at a distance representative of the three-way catalyst position downstream of the engine at a 2 bar net indicated mean effective pressure (NIMEP) steady-state operating condition representative of cold-start. The test matrix included sweeps of ignition timing 15 degrees-before to 10 degrees-after top dead center firing (TDC_f) across three different spark-plug heat dispersal ranges (HR). Additionally, the effect of varying exhaust valve opening (EVO) timing on combustion stability and emissions was also studied. Results show that the spark plug HR affects the coefficient of variation (COV) of NIMEP under all cold-start conditions, while the impact on emissions was found to be minimal. At very retarded spark timings, colder spark plugs required higher air and fuel flow to maintain the desired 2bar NIMEP load, but the fraction of fuel energy going into the exhaust was found to be similar for all spark plugs. Retarding exhaust valve timings showed a simultaneous reduction in emissions while increasing the fraction of fuel energy being fed into the exhaust. However, engine COV was also observed to increase with retarded exhaust timings.

Introduction

With improving aftertreatment system performance under warm conditions, cold-start operation which is defined as time between first-crank and three-way-catalyst light-off is emerging as the dominant source of pollutant emissions such as NOx, unburned hydrocarbons (HC), and particulate matter mass (PM) and particulate matter number (PN) [1 - 4]. Acknowledging this trend, improvement in understanding and prediction of cold start operation through generation of detailed experimental data as well as modeling capabilities forms a major pillar of US Department of Energy's partnership for advancing combustion engines (PACE) initiative [5]. Cold start operation in light-duty spark-ignited engines has been the focus of multiple experimental [5 - 15] and computational [16 -19] studies in literature.

Rodriguez et. al. have published numerous studies detailing experimental investigation of various aspects of cold-start operation in a modern direct-injection spark-ignition (DISI) gasoline engine under both cold-cranking as well as cold fast idle (1200RPM 2bar NIMEP) conditions [6, 8, 10]. In a study aimed at understanding cold cranking emissions [6], the authors observed an order of magnitude reduction in PM emissions as the crank-start progressed from the first firing cycle to the third firing cycle, however, HC emissions remained unchanged across the first three cycles. In a subsequent study [8], the authors investigated the effect of valve timing during both cold crank start and cold fast idle operation and observed that retarding intake valve opening provided more than 25% reduction in both HC and PM emissions during cold crank start while retarding exhaust cam phasing also reduced HC and PM emissions. However, at cold-fast idle, retarding exhaust cam phasing resulted in increased HC and PM emissions. Finally, combining late intake valve opening and early exhaust valve closing with moderate combustion phasing retard provided the best compromise between HC/PM emissions and engine stability. Finally, in another similar study aimed at understanding NOx emissions [10], the authors observed strong dependence of cold-start NOx emissions on combustion phasing. NOx was observed to decrease for moderately retarded combustion phasing (up to CA50 of 40 degrees after TDCf) but started to increase again as combustion phasing was further retarded. An increase in fuel flow and a reduction in combustion residuals were hypothesized as the main contributing factors for this observation.

Etikayla et. al. [13] analyzed the effect of start-of-injection (SOI) timing on cold-start PN emissions in a DISI engine and observed that SOI played a significant role in PN emissions with retarded SOI timings producing lower PN emissions. Accompanying in-cylinder endoscopic imaging corroborated these findings and identified piston-wetting as the main source of PN emissions.

The aim of this study is to understand the effect of engine parameters such as spark plug heat range (HR), exhaust valve timing, and spark timing on engine emissions and cycle-to-cycle variation under cold-start operation. This study expands the envelope of combustion phasing, exhaust heat flux, and exhaust valve timing values beyond what has previously been reported in literature for cold-start operation and provides data for edge cases, critical for validation of

computational models and study of cyclic variability properties of cold-start operation. The results shown try to elucidate the mechanisms of HC and particulate formation and narrow down conditions for further study with advanced diagnostic techniques and high-fidelity simulations.

Experimental Setup

This study utilizes a single-cylinder version of a GM LNF 2.0L DISI engine, wherein 3 of the cylinders were disabled by removing the cam lobes as well as drilling holes in the pistons to prevent compression. The firing cylinder was run in stock configuration, wherein compression ratio, combustion chamber geometry, fuel injector, cam lobe profiles and cam phasing capabilities were all stock. Furthermore, stock high-pressure gasoline fuel pump, fuel rail, and oil pump were also retained. Engine specifications are listed in Table 1. The engine features extensive instrumentation (Figure 1) including high-speed transducers for intake port (Kistler 4007D), in-cylinder (Kistler 6125c), and exhaust port (Kistler 4049B) pressure measurements as well as various thermocouples for temperature measurements. Fuel flow was measured using a Coriolis flow meter. A combination of an external standalone air-compressor and a mass flow controller (Alicat MCR) was utilized to feed desired air flow into the engine. Intake and exhaust surge tanks were utilized to dampen pressure pulses. Exhaust gas concentrations were measured using standard gas analyzers, i.e., non-dispersive infrared analyzers for CO_2 and CO, a paramagnetic analyzer for O_2, a flame ionization detector for unburned hydrocarbons (HC), and a chemiluminescent detector for NO_x measurements. The exhaust gas emissions sampling port was located at 200mm distance from the exhaust port outlet. Soot was measured using a AVL micro-soot sensor. Three 1/8" K-type thermocouples were placed along the exhaust manifold length at 25mm, 100mm, and 200mm from the exhaust port to track exhaust gas temperature evolution in the manifold. Finally, an external chiller was utilized to maintain engine-out oil and coolant temperatures at 20°C.

The PACE consortium is focused on market-representative fuels. Consequently, for this study the engine was operated on an E10 regular-grade research gasoline from Halterman (product name RD5-87, fuel properties listed in Table 2), and fuel effects are out of the scope of this work. Measurements were taken during stoichiometric steady-state engine operation at 1300RPM and 2bar NIMEP. This speed/load condition was finalized as a steady-state surrogate for cold start operation research by the USDRIVE advanced combustion and emission control (ACEC) tech team, which included inputs from the US light-duty-engine original equipment manufacturers (OEMs). Air flow and fuel flow were set for each case to achieve engine-out stoichiometric operation at 2 bar NIMEP load. Air-fuel ratio was calculated from intake and exhaust gas analyzer measurements using the LabVIEW version of the Engine Emissions & Uncertainty Analysis code by Dempsey and Ghandhi [20]. Furthermore, lambda calculated from exhaust emissions measurements was used to control engine stoichiometry. Engine control was provided by a National Instruments Powertrain Controls Engine Control System (ECS) that is capable of next-cycle control action, with the integrated in-house Oak Ridge Combustion Analysis System (ORCAS) performing heat release and other combustion analysis calculations.

Impact of engine parameters such as spark plug HR, and exhaust valve opening (EVO) timing on steady-state cold-start engine performance was independently assessed using spark timing sweeps from -15 to 10 crank angle degrees after top dead center of firing (ATDCf). Fuel injection timing was maintained at -280° ATDCf for all conditions at an injection pressure of 120 bar.

For the spark plug HR study, spark sweep data was taken using commercially available Denso spark plugs with heat ranges of 16 (ITV16), 22 (ITV22), and 24 (ITV24). HR16 spark plug has the lowest heat dispersal capability and is the stock application for this engine. The HR16, and HR22 spark plugs have the same reach, while the HR24 spark plug has a 2mm shorter reach. While spark plugs with a higher heat dispersal capability provide knock and pre-ignition benefits at higher loads, this study aims to understand if cold-start performance and cycle-to-cycle variability is also sensitive to spark plug HR. For the EVO timing study, cold-start performance was analyzed at exhaust cam phasing of 0, 25, and 50 crank angle degrees (CAD) at three spark timings (-10, 0, and 10 dATDCf). Increasing exhaust cam phasing retards EVO timing. The intake cam was fixed at 0 CAD phasing. Maximum negative valve overlap (NVO) was achieved when both intake and exhaust cams have 0 phasing.

Table 1: Engine Specifications

Bore	86 mm
Stroke	86 mm
Configuration	I-4 (single)
Compression Ratio	9.2:1
Ignition Coil Energy	80 mJ
Induction	Air compressor via air-mass flow controller
Fuel System	Side-mount gasoline direct injection

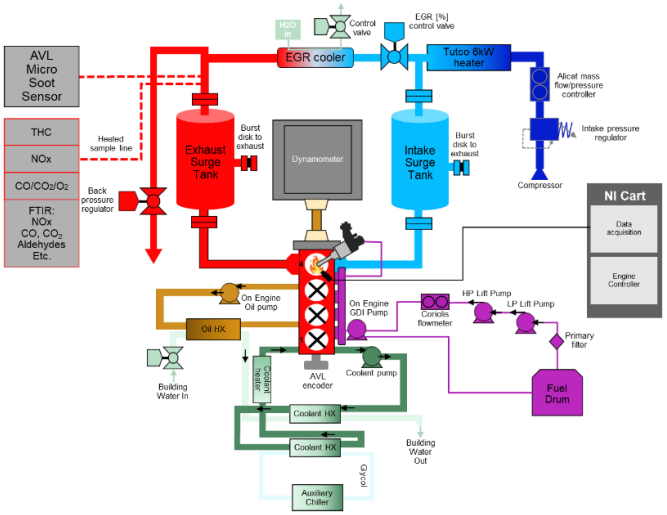

Figure 1: Single-Cylinder Engine System Diagram

Table 2: RD5-87 E10 Gasoline Fuel Properties

Research Octane Number [-]	ASTM D2699	92.3
Motor Octane Number [-]	ASTM D2700	84.6
Octane Sensitivity [-]	RON – MON	7.7
Initial boiling point [°C]	ASTM D86	40.4
T10 [°C]	ASTM D86	54.8
T50 [°C]	ASTM D86	101.3
T90 [°C]	ASTM D86	157.9
Final boiling point [°C]	ASTM D86	172.1
Specific Gravity [-]	ASTM D4052	0.75
Carbon [wt %]	ASTM D5291	82.67
Hydrogen [wt %]	ASTM D5291	13.66
Oxygen [wt %]	ASTM D5599	3.51
Stoichiometric Air-Fuel Ratio	Calculated	14.2
Lower Heating Value [MJ/kg]	ASTM D4809	41.93
Aromatics [wt %]	ASTM D6729	27.9
n-Saturates [wt %]	ASTM D6729	13.9
Iso-Saturates [wt %]	ASTM D6729	29.0
Olefins [wt %]	ASTM D6729	5.5
Naphthenes [wt %]	ASTM D6729	12.4
Ethanol [wt %]	ASTM D5599	10.12

Results and Discussion

Effect of Spark Timing on cold-start performance

Engine operation was evaluated at cold-start relevant spark timings ranging from -15 to 10 CAD ATDCf and results are detailed in Figure 2. As expected, retarded spark timings required higher air and fuel mass flow rates to maintain the desired load due to loss of gross efficiency (Figure 2a), while retarded spark timings also exhibited a sharp decrease in combustion stability as measured by the coefficient of variation (COV) of NIMEP. Significant exhaust temperature increase (~200 ºC) was observed with spark timing retard (Figure 2b), which coupled with increased air flow produced almost 4 times higher exhaust heat rate (Figure 2c). The fraction of fuel energy being ejected into the exhaust also increased by ~50% across the swept spark timing range. The fraction of fuel energy ejected into the exhaust was tracked using a '% Fuel Energy in Exhaust' variable which was calculated as per Eq. 1

$$\%\ Fuel\ Energy\ in\ Exhaust = \frac{Exhaust\ Heat\ Rate}{Fuel\ Flow\ Rate \times LHV} \times 100 \qquad \text{Eq. 1}$$

HC emissions were observed to monotonically decrease with spark retard, with ~75% reduction in HC mass flux observed across the spark timing sweep (Figure 2d). This is believed to be a result of higher exhaust temperatures and the associated increase in post-exhaust oxidation of HC in the exhaust pipe before measurement. Conversely, NOx emissions exhibited an initial reduction with spark retard followed by increase at even later spark timings (Figure 2d). This behavior is similar to previous studies [10]. The initial decrease in NOx is due to a delay on the crank angle of 50% mass fraction burned (CA50) and lower in-cylinder temperatures. However, beyond a certain CA50, an increase in bulk in-cylinder temperature (Figure 2f), mainly due to significantly higher air and fuel mass flow rates required to maintain engine load, caused NOx to reverse trends and increase for further spark retard. Fuel-mass normalized HC and NOx emissions also exhibited similar trends as shown in Figure 2e. Finally, higher exhaust temperatures are expected to cause a reduction in trapped residuals which will result in higher NOx emissions per unit fuel mass and likely contribute to the observed trends.

Loss of fuel to engine oil was tracked across the spark timing sweep using the λ_{ratio} parameter as defined in Eq 2.

$$\lambda_{ratio} = \frac{\lambda_{mass}}{\lambda_{emissions}} \qquad \text{Eq. 2}$$

where, λ_{mass} is the air-fuel equivalence ratio calculated using air and fuel mass flows and $\lambda_{emissions}$ is the air-fuel equivalence ratio calculated from emissions measurements. If no fuel is lost to engine oil, then λ_{ratio} would be close to 1. However, if fuel is being lost to engine oil, then the additional fuel required to compensate for this fuel loss will cause λ_{mass} calculation to go rich, i.e., less than 1, while $\lambda_{emissions}$ would still be controlled to stochiometric, i.e., at 1. The measured λ_{ratio} is shown in Figure 3 and was observed to decrease with retarded spark timing indicating increasing fuel loss to engine oil with spark retard.

It is likely that the increase in fuel loss indicated by this metric is caused by the increased injection duration as spark is retarded. Other factors such as in-cylinder density at the time of injection and residence time between injection and spark are also likely contributors, due to complex spray dynamics, film formation and oil absorption/desorption effects. Ravindran [19] showed through computational fluid dynamic (CFD) simulations that most of the fuel wall film is formed at the piston surface. However, their simulation results suggested that increased wall-film formation would translate into higher HC emissions. In the case of the current experiments this is not observed. As described previously, HC emissions monotonically decreased with retarded spark timings. However, due to computational limitations, their results did not consider a constant engine load which likely skews the results. Additionally, a major difference between the computations and experiments is that simulations by Ravindran did not include a representative exhaust manifold domain which is expected to have a significant impact on the measured HC emissions due to post combustion oxidation. Finally, as shown in Figure 3, soot emissions were observed to sharply increase at retarded spark timings which indicates portions of the rich wall film formed during and after the injection event were converted to soot and did not contribute to HC emissions as Ravindran's [19] results suggested. In the current experiments it is unclear whether wall-film formation was increased by the changes in spark timing, fueling and airflow, and the increased soot could also stem from prolonged exposure of the fuel to a hotter environment during the slow combustion rates prevailing at very retarded spark timings, instead of increased wall film masses.

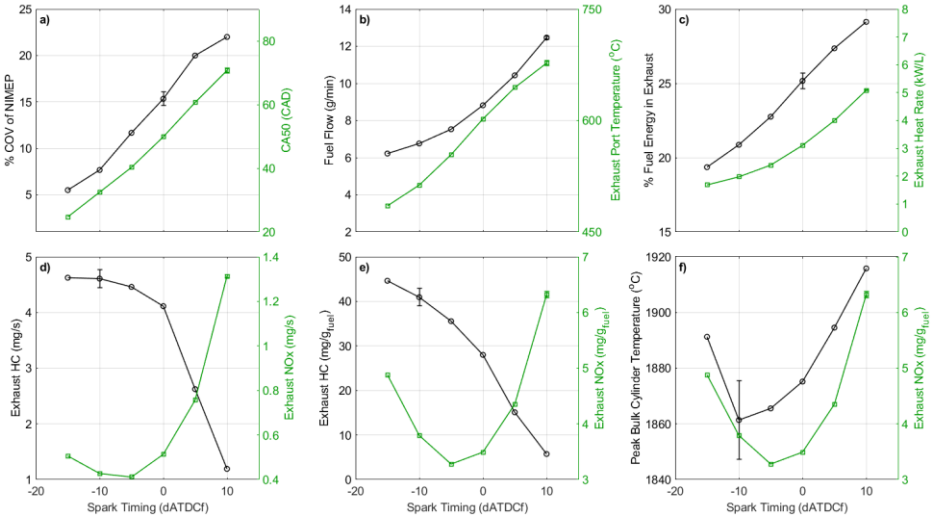

Figure 2: Effect of spark timing on cold-start performance at 1300 RPM and 2 bar NIMEP stoichiometric operation. Results show an increase in COV as spark timing is retarded coupled with increased fuel flow to meet the engine-load setpoint. Significant increases in exhaust heat rate were also observed. HC emissions fall monotonically with spark retard, but NOx emissions exhibit a non-monotonic behavior. (Note: Error bar represents average of uncertainty observed across all data points of the respective data series and is only shown on one data point of each series to reduce clutter and improve graph readability)

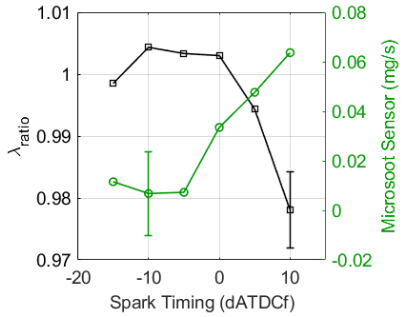

Figure 3: λ_{ratio} and soot measurements during 1300 RPM and 2 bar stoichiometric operation across a spark timing sweep. Decreasing λ_{ratio} at retarded spark timings indicate increased fuel-loss to oil. (Note: Error bar represents average of uncertainty observed across all data points of the respective data series and is only shown on one data point of each series to reduce clutter and improve graph readability)

Effect of Spark Plug Heat-Range on Cold-Start Performance

Figure 4 shows the cold-start performance with the three spark plug HRs across the spark timing sweep as well as a function of the achieved exhaust heat rate. For expediency the spark plug with the lowest heat dispersal capability will be referred to as the hot spark plug, and conversely the highest heat dispersal spark plugs will be referred to as cold.

Combustion stability, as measured by COV of NIMEP was observed to improve with increasing spark plug heat range where the hottest spark plug (HR16) consistently presented lower COV than the colder plugs. It is likely that hotter spark plug conditions aided in reducing the variability of the kernel formation and development process, thereby decreasing cycle-to-cycle variability. Further, at more retarded spark timings where combustion becomes increasingly challenging, the colder spark plugs required higher air and fuel flows to maintain engine load. However, as a direct result of this increased air flow requirement, the colder spark plugs also produced higher heat rate in the exhaust, proportional to the increase in fuel flow, but nevertheless not particularly significant. Hydrocarbon emissions were observed to be similar for all three spark plugs. The coldest spark plug (HR24) produced ~25% higher NOx emissions at retarded spark timings. It should be noted the differences observed between HR22 and HR24 spark plugs are significantly larger than those observed between the HR22 and HR16 plugs, and it is possible that in addition to the colder heat range, the shorter reach of the HR24 spark plug could be an additional impediment to combustion stability. As observed in Figure 4a – 4c differences exist in the combustion stability and NOx emissions of the three spark plugs; however, when analyzed in exhaust heat rate (or fuel flow) domain as shown in Figure 4 d) – e), some of the trends converge. For catalyst heating purposes, exhaust heat rate is a more relevant metric as engine controllers will try to adjust engine parameters such that the highest exhaust heat rate is achieved while meeting combustion stability metrics to allow for fastest catalyst heating. Figure 4d shows that the hotter spark plug (HR16) provides better combustion stability for a given exhaust heat rate. For a given COV of NIMEP limit the hottest spark plug, which showed improved stability, would likely reach higher exhaust heat rates due to the direct correlation between COV of IMEP and exhaust heat rates. For example, for a 20% COV of IMEP limit, both HR22 and HR24 would reach exhaust heat rates of ~2.8 kW/L while HR16 would allow ~3.8 kW/L heat rates under the current conditions. Conversely, the spark plug heat range does not appear to play a role in other metrics such as exhaust temperature, % of fuel energy in exhaust, HC and NOx emissions. All metrics were observed to follow the same trend line vs exhaust heat rate, indicating that larger spark retard is required with hotter spark plugs to achieve a desired exhaust heat rate. Further, as shown in Figure 5, λ_{ratio} trends were consistent across the three spark plugs and were not statistically significant given the uncertainty of the current measurements as illustrated by error bars in Figure 5.

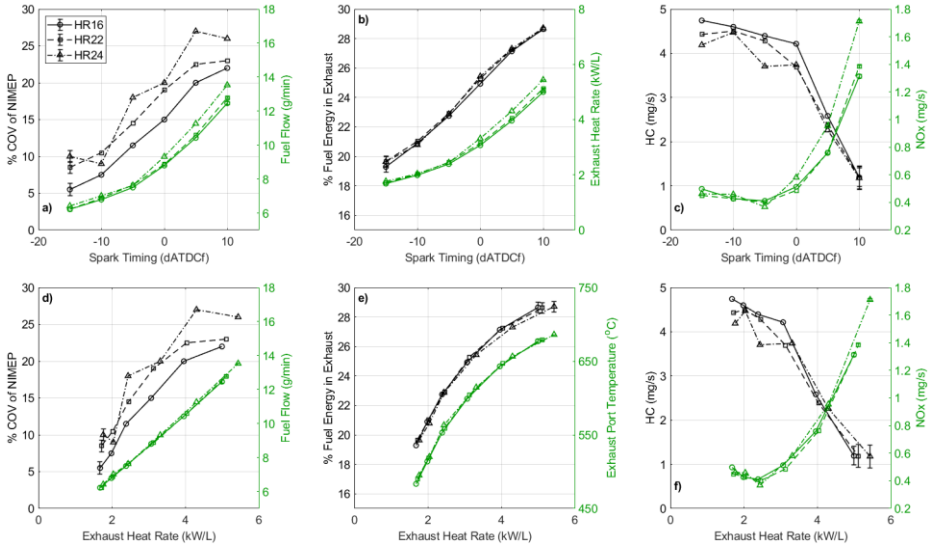

Figure 4: Effect of spark plug heat range (HR) on cold-start performance at 1300 RPM and 2 bar NIMEP stoichiometric operation. Results show that while some differences exist across the performance of the three spark plugs, most trends are consistent across the three plugs when analyzed in the exhaust heat rate space. COV is the only performance parameter where differences exist with the hotter spark plug (HR16) exhibiting a lower COV. (Note: Error bar represents average of uncertainty observed across all data points of the respective data series and is only shown on one data point of each series to reduce clutter and improve graph readability)

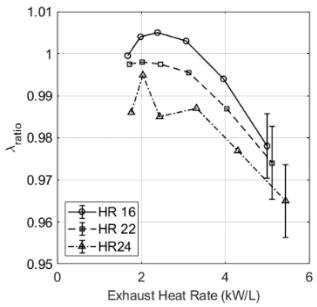

Figure 5: λ_{ratio} measurements during 1300 RPM and 2 bar stoichiometric operation across a spark timing sweep for three spark plug heat ranges (HR16, HR22, and HR24). Decreasing λ_{ratio} at retarded spark timings indicate increased fuel-loss to oil. Similar trends observed for all spark plugs, and difference between the trends of the three spark plugs not statistically significant for the current study. (Note: Error bar represents average of uncertainty observed across all data points of the respective data series and is only shown on one data point of each series to reduce clutter and improve graph readability)

Effect of Exhaust Cam Timing on Cold-Start Performance

Cold start performance was assessed at three different exhaust cam phasing timings (0, 25, and 50 CAD EVO retard) and at three different spark timings. The engine was run in steady state at 1300 RPM and 2 bar NIMEP with the HR16 spark plug. As shown in Figure 6, for all three spark timings, EVO retard resulted in significant combustion phasing retard as well as a sharp increase in COV of NIMEP. Significantly higher fuel (and air) flow was required to meet the 2 bar NIMEP setpoint (Figure 6b) as EVO was retarded from the baseline with ~90% fuel flow increase observed at all three spark timings. EVO retard also provided a significant boost to the exhaust heat rate over the baseline cam timing for all spark timings tested. While some of this increase could be attributed to the increase in fueling, as shown in Figure 6e, EVO retard also increases the fraction of fuel energy being ejected into the exhaust stream at all three spark timings. Furthermore, the effect of EVO retard on % of fuel energy in exhaust was observed to be a uniform ~35% increase for all three spark timings. Emissions of HC and NOx were observed to decrease with EVO retard for all spark timings in both the absolute mass flow space (Figure 6c) as well as the fuel-mass normalized space (Figure 6f). Simulations by Ravindran [19] showed a reduction in NOx and HC emissions as EVO was delayed and valve overlap was increased, agreeing with the current results. Their simulation results, and the current hypothesis based on the experimental data presented in this study suggest that the HC and NOx emissions reductions under delayed EVO conditions are related to two distinct effects: (1) Delaying EVO and increasing valve overlap will increase the amount of trapped residual gases and promote exhaust rebreathing, as indicated by the increased fuel and airflow requirements to maintain load and stoichiometry (Figure 6b), (2) A delay in EVO timing allows more time for fuel films to evaporate and be oxidized in the cylinder environment. Increased trapped residuals will lead to lower peak cylinder temperatures and therefore lower NOx emissions. While both increased exhaust rebreathing and film evaporation will enhance HC oxidation.

The HC emissions trends observed in this study are the opposite of previous observations [8]. However, there are critical differences in the boundary conditions applied in both experiments. First, fuel injection pressure and start of injection timing were lower and more retarded, respectively. Consequently, differences in the spray dynamics and wall wetting characteristics are expected, which may be the source of the discrepancy between the trends. Perhaps most importantly, the results from Rodriguez [8] were conducted with no valve overlap, even at the latest EVO. The difference in the pressure balances caused by the lack of overlap likely prevents the rebreathing of the exhaust which is believed to be the main contributor to HC oxidation and its reduction as EVO is delayed. Nevertheless, currently sufficient information does not exist to draw definitive conclusions on the specific causes of the differences observed in trends, and detailed simulations or advanced diagnostic measurements are required to provide more clarity.

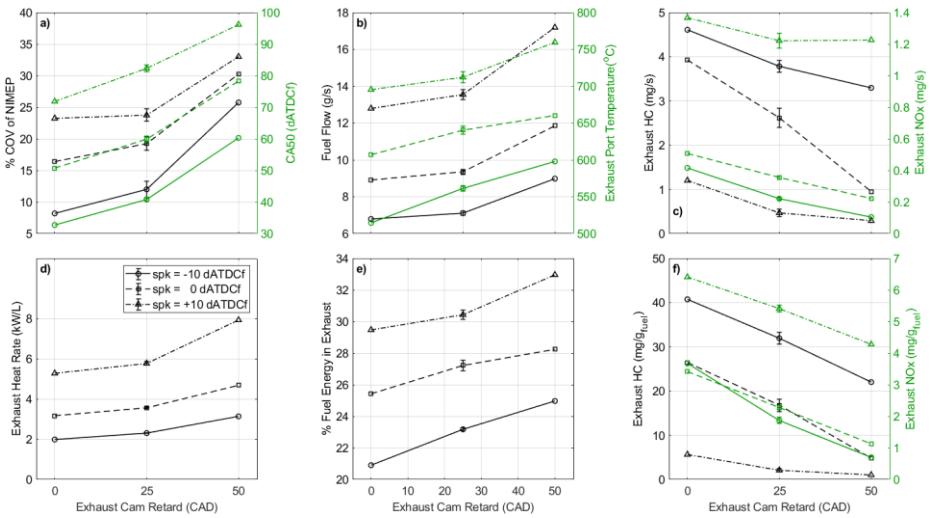

Figure 6: Effect of exhaust valve opening (EVO) timing on cold-start performance at 1300 RPM and 2 bar NIMEP stoichiometric operation. Exhaust cam retard delays EVO timing and a set of three cam retard timings are shown for three spark timings. Results show an increase in COV as exhaust cam is retarded, coupled with increased fuel flow to meet the engine-load setpoint. Significant increases in exhaust heat rate also observed. Both HC and NOx emissions fall monotonically with exhaust cam retard. (Note: Error bar represents average of uncertainty observed across all data points of the respective data series and is only shown on one data point of each series to reduce clutter and improve graph readability)

In previous sections, fuel loss was observed to increase with retarded spark timings. However, both the total fueling as well as peak compression pressure (due to increased air flow) also increased with spark retard to compensate for the loss of efficiency due to retarded combustion phasing. Therefore, spark timing, total fueling, and compression pressure could all play a role in impacting fuel-loss to oil. As shown in Figure 6b, retarding EVO timing increases fueling and therefore compression pressures (due to increased air flow) even for a fixed spark timing. Therefore, λ_{ratio} trends across EVO timing sweeps could shed light on the contributions of increase in fueling and compression pressure to fuel loss. Figure 7 shows λ_{ratio} trends at three different spark timings as well as three exhaust cam phasing timings. As spark timing is changed, the λ_{ratio} trends are consistent with findings of previous sections, i.e., λ_{ratio} reduces at retarded spark timings indicating higher fuel-loss to oil. However, for a given spark timing, the λ_{ratio} does not change even though total fueling, and compression pressures are increasing significantly due to EVO timing retard. This indicates that either spark timing is the major factor in fuel-loss to oil through a yet unknown mechanism or that EVO timing retard is counteracting the effect of increasing fueling and compression pressures. As explained previously, it is likely that the longer residence time of the cylinder gases and higher temperatures at EVO allow more time for film evaporation. This is in contrast with the results in Figure 3 where it was hypothesized that the increased injection durations were responsible for the increased fuel losses to oil and increases in soot. Figure 8 shows soot measurements for the EVO timing experiments. It is evident that EVO timing retard leads to a substantial increase in soot emissions. It is likely that film formation is still increased with EVO timing retard, but fuel is being deposited in large quantities on the piston surface and away from the oil film, and thereby forming soot rather than being absorbed by the oil and exiting the system. Consequently, fuel film formation and fuel-oil losses should not be conflated, and more detailed investigations are needed to elucidate all possible contributing factors such as in-cylinder density, injection spray characteristics, film dynamics and evaporation, and exhaust rebreathing. While EVO timing retard increases valve overlap, the increase in air flow also leads to a reduction in the engine delta-pressure as shown in Figure 9. This finding warrants further investigation as exhaust cam phasing could be an attractive option to increase exhaust heat rate while incurring a lower fuel-loss penalty and is shown to provide favorable trends if there is positive valve overlap due to rebreathing.

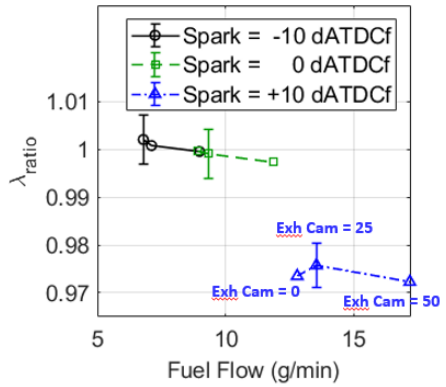

Figure 7: λ_{ratio} measurements during 1300 RPM and 2 bar stoichiometric operation at three exhaust cam phasing timings and three spark timings. The three line groups indicate the three different spark timings, and the three points in each line group represent data for a cam phasing timing. For all spark timings, fuel flow was observed to increase with exhaust cam retard. (Note: Error bar represents average of uncertainty observed across all data points of the respective data series and is only shown on one data point of each series to reduce clutter and improve graph readability)

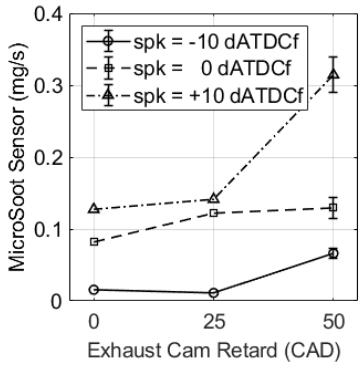

Figure 8: Soot measurements during 1300 RPM and 2 bar stoichiometric operation at three exhaust cam phasing timings and three spark timings. For all spark timings, a general trend of increase in soot with exhaust cam retard is observed. (Note: Error bar represents average of uncertainty observed across all data points of the respective data series and is only shown on one data point of each series to reduce clutter and improve graph readability)

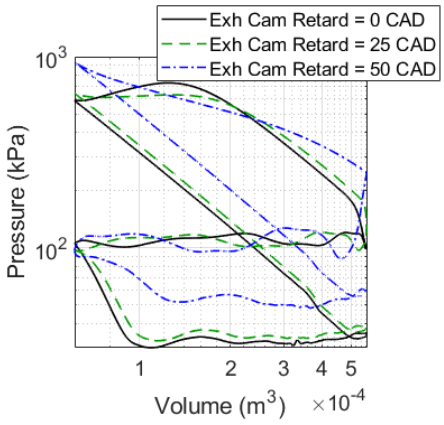

Figure 9: Cycle-averaged logP-logV diagrams for 1300 RPM and 2 bar stoichiometric operation at three different exhaust cam retard timings. Spark timing was -10 CAD ATDCf. Trends indicate reduction in engine delta-pressure as exhaust cam is retarded.

Figure 10 shows the evolution of gas temperature measured along the exhaust manifold length using three thermocouples installed at 25mm, 100mm, and 200mm from the exhaust port. Under normal engine operation, when most of fuel oxidation occurs in the cylinder, a drop in gas temperature is expected because of heat transfer losses to the exhaust manifold as well as surroundings. Any deviations from this trend would indicate presence of oxidation reactions in the exhaust stream (outside of the cylinder). Figure 10a shows the temperature evolution when the exhaust cam phasing is zero. While the expected trend of temperature reduction is observed at advanced spark timings (-10 and 0 CAD ATDCf), at the most retarded spark timing of 10 CAD ATDCf the temperature initially increases slightly before starting to reduce. This indicates that at 10 CAD ATDCf ignition timing, the combustion phasing is retarded enough that oxidation reactions are still occurring in the exhaust even after gases exit the exhaust port. Adding EVO retard further delays combustion phasing (Figure 6a), leading to increased oxidation in the exhaust. This is especially apparent at an exhaust cam retard of 50° (Figure 10c) wherein even at an ignition timing of 0 CAD ATDCf the result exhibits a flat temperature profile while at an ignition timing of 10 CAD ATDCf the temperature is continuing to rise even 200mm downstream of the exhaust port indicating the presence of significant oxidation reactions in the exhaust manifold. The presence of oxidation reactions in the exhaust manifold also potentially contributes to the emissions trends observed in Figure 6c and Figure 8. Continuation of oxidation in the exhaust likely leads to longer residence times of unburned HC in a hot environment which could further strengthen HC oxidation and/or soot formation

mechanisms. Characterizing the nature of these reactions and its products will provide valuable information for cold-start modeling efforts.

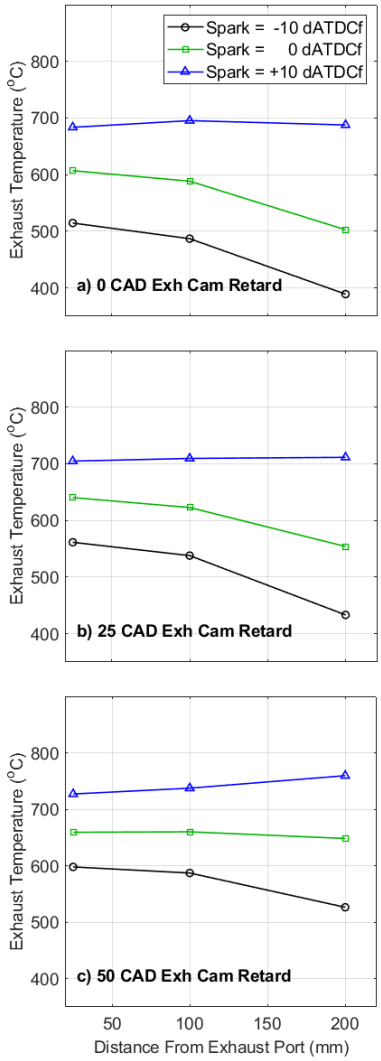

Figure 10: Temperature evolution in the exhaust manifold at exhaust cam phasing of 0, 25, and 50 CAD and at spark timing of -10, 0, and 10 CAD ATDCf. Trends indicate presence of oxidation reactions in the exhaust manifold at later combustion phasing conditions.

Conclusions

Impact of engine control variables such as spark timing retard, spark plug heat range, and exhaust valve timing retard were documented at cold-start relevant steady-state operation of a direct-injected spark-ignited engine fueled by a market-representative E10 gasoline fuel. Engine performance was characterized using parameters such as COV, fuel-loss-to-oil, exhaust heat rate, soot and HC/NOx emissions.

Spark timing retard caused a retarded CA50 and increased the exhaust heat rate. Retarding EVO was observed to further increase the exhaust heat rate and this effect was observed to be uniform across all investigated spark timing values. Ultimately, an exhaust heat rate of ~8kW/L was achieved when both spark and EVO timing were retarded simultaneously. The increase exhaust heat rate makes spark and EVO retard attractive as cold-start catalyst heating strategies. However, the increase in exhaust heat rate was also accompanied by decreased engine stability as evidenced by the increased COV of NIMEP values. Therefore, practical cold-start strategies would be required to implement a compromise between the desired exhaust heat rate and engine stability.

NOx initially decreases with spark retard, but trends reverse beyond a certain CA50 level. This is due to increases in the required fuel and air flows, for maintaining a constant engine load, resulting in higher in-cylinder temperatures and lower residual gas trapping; both of which contribute to increased NOx emissions

HC emissions monotonically decrease with spark retard. This is counter to the expectation that poor combustion performance at later spark timings would result in higher unburned fractions. However, emissions measurements were performed 200 mm downstream of the engine allowing time for post-exhaust oxidation of HC. At retarded timings this was shown to be more prevalent due to higher exhaust temperature conditions. Temperature measurements along the exhaust reinforced presence of heat release in the exhaust pipe.

Spark plug heat range affects combustion stability but no other metric, i.e., for a given COV of NIMEP limit hotter spark plugs can enable higher exhaust heat rates.

Spark retard caused an increase in fuel loss as measured by mass- and emissions-based lambdas indicating higher losses of fuel to the oil. This is expected to be caused by increased injection durations required for maintaining a constant engine load across the spark timing sweep range. Other factors such as in-cylinder density at the time of injection and residence time between injection and spark are also likely contributors, due to complex spray dynamics, film formation and oil absorption/desorption effects. EVO timing sweeps suggested there may be competing effects that contribute to higher fuel loss and higher soot emissions, which needs to be further investigated.

Delaying the EVO timing resulted in favorable emissions trends with a reduction in HC and NOx likely due to exhaust rebreathing caused by the increased valve overlap. However, soot emissions were measured to increase as EVO was delayed and the increases were more substantial at the most delayed spark timing where exhaust heat rates are higher. Simulation results by Ravindran [19] support these findings. Nevertheless, previous experimental results by Rodriguez [8] showed the reverse trend for HC emissions. Their experiments were conducted without positive valve overlap which is hypothesized to enable exhaust rebreathing and oxidation of unburned HCs. Additionally, boundary conditions such as fuel injection pressure and fuel injection timing were different and may significantly affect spray dynamics and fuel wall film formation. Additional investigations using CFD and advanced diagnostics are needed to isolate the principal effects causing a reversal in emissions trends.

Future work could involve investigation of other engine control variables such as split-injection strategies which could potentially change the fuel-loss and soot trends observed here through changes in spray penetration and wall/piston wetting. Another possible future work could involve investigation of the effect of fuel properties on cold-start performance and emissions. Fuel properties such as distillation and heat-of-vaporization will likely impact both spray penetration as well as vaporization of liquid fuel from the walls/crevices therefore impacting the fuel-loss and soot trends, while properties such as ignition delay are likely to impact HC oxidation in crevice regions.

References

[1] Chen, Hai-Ying, and Chang Hsiao-Lan (Russell). “Development of Low Temperature Three-Way Catalysts for Future Fuel

Efficient Vehicles." Johnson Matthey Technology Review 59(1), (2015): 64-67. doi:10.1595/205651315X686011.

[2] Myung, Cha-Lee, Kim Juwon, Jang Wonwook, et al. "Nanoparticle Filtration Characteristics of Advanced Metal Foam Media for a Spark Ignition Direct Injection Engine in Steady Engine Operating Conditions and Vehicle Test Modes." Energies 8(3), (2015): 1865-81. doi:10.3390/en8031865.

[3] Chambon, P., Deter, D., Irick, D. and Smith, D., "PHEV Cold Start Emissions Management," SAE Int. J. Alt. Power. 2(2):2013, doi:10.4271/2013-01-0358..

[4] Qi Liu, Jingping Liu, Jianqin Fu et. al. "Comparative study on combustion and thermodynamics performance of gasoline direct injection (GDI) engine under cold start and warm-up NEDC," Energy Conversion and Management 181, (2019): 663-673. https://doi.org/10.1016/j.enconman.2018.12.043.

[5] McNenl M, Miles PC, Som S, and Szybist JP. "Partnership for Advanced Combustion Engines (PACE) - A Light-Duty National Laboratory Combustion Consortium, " United States: N. p., 2020. Web. https://www.energy.gov/node/4448704

[6] Rodriguez, J. and Cheng, W., "Cycle-by-cycle analysis of cold crank-start in a GDI engine," SAE Int. J. Engines 9(2):2016, doi:10.4271/2016-01-0824.

[7] Fedor, W., Kazour, J., Haller, J., Dauer, K. et al., "GDi Cold Start Emission Reduction with Heated Fuel," SAE Technical Paper 2016-01-0825, 2016, doi:10.4271/2016-01-0825.

[8] Rodriguez, J. and Cheng, W., "Reduction of Cold-Start Emissions through Valve Timing in a GDI Engine," SAE Int. J. Engines 9(2):2016, doi:10.4271/2016-01-0827.

[9] Badshah, H., Kittelson, D., and Northrop, W., "Particle Emissions from Light-Duty Vehicles during Cold-Cold Start," SAE Int. J. Engines 9(3):2016, doi:10.4271/2016-01-0997.

[10] Rodriguez, J. and Cheng, W., "Analysis of NOx Emissions during Crank-Start and Cold Fast-Idle in a GDI Engine," SAE Int. J. Engines 10(2):2017, doi:10.4271/2017-01-0796.

[11] Hu, J., Hall, M., Matthews, R., Moilanen, P. et al., "A Novel Technique for Measuring Cycle-Resolved Cold Start Emissions Applied to a Gasoline Turbocharged Direct Injection Engine," SAE Int. J. Advances & Curr. Prac. in Mobility 2(5):2469-2478, 2020, doi:10.4271/2020-01-0312..

[12] Jaworski, A., Mądziel, M., Kuszewski, H., Lejda, K. et al., "Analysis of Cold Start Emission from Light Duty Vehicles Fueled with Gasoline and LPG for Selected Ambient Temperatures," SAE Technical Paper 2020-01-2207, 2020, doi:10.4271/2020-01-2207.

[13] Etikyala, S. and Dahlander, P., "Soot Sources in Warm-Up Conditions in a GDI Engine," SAE Technical Paper 2021-01-0622, 2021, doi:10.4271/2021-01-0622.

[14] Abdulfatah Abdu Yusuf, Freddie L. Inambao. "Effect of cold start emissions from gasoline-fueled engines of light-duty vehicles at low and high ambient temperatures: Recent trends," Case Studies in Thermal Engineering 14, (2019). https://doi.org/10.1016/j.csite.2019.100417.

[15] Longfei Chen, Zhirong Liang, Xin Zhang, Shijin Shuai. "Characterizing particulate matter emissions from GDI and PFI vehicles under transient and cold start conditions," Fuel 189, (2017): 131-140. https://doi.org/10.1016/j.fuel.2016.10.055.

[16] Kim, Sung-Jun and Hyun, Soungjae and Park, JaeIn, "Optimization of Cold Start Operating Conditions in a Stoichiometric GDI Engine with Wall-guided Piston using CFD Analysis," SAE Technical Paper 2013-01-2650. (2013) https://doi.org/10.4271/2013-01-2650.

[17] Asami, S. and Shiraishi, T., "Availability of Balanced Truncation for Reducing an Automotive Cold Start Engine Model," SAE Int. J. Engines 9(2):2016, doi:10.4271/2016-01-9152.

[18] Ravindran, Arun C, Sage L Kokjohn, and Benjamin Petersen. "Improving Computational Fluid Dynamics Modeling of Direct Injection Spark Ignition Cold-Start." International Journal of Engine Research, (October 2020). https://doi.org/10.1177/1468087420963982.

[19] Ravindran A. "Numerical Modeling of Gasoline Direct Injection Spark Ignition Engines during Cold-Start," PhD Thesis, University of Wisconsin (2021).

[20] Dempsey A, Ghandhi J. "Engine Emissions & Uncertainty Analysis," [Online].; 2015 [cited 2015 12 29]. Available from: http://sourceforge.net/projects/engine-emissions-uncertainty/files/.

Contact Information

Gurneesh S. Jatana
National Transportation Research Center
Oak Ridge National Laboratory
2360 Cherahala Boulevard
Knoxville, TN 37932
jatanags@ornl.gov

Acknowledgments

This research was conducted as part of the Partnership to Advance Combustion Engines (PACE) Consortium sponsored by the U.S. Department of Energy (DOE) Vehicle Technologies Office (VTO). The PACE Consortium is a collaborative project of multiple National Laboratories that combines unique experiments with world-class DOE computing and machine learning expertise to speed discovery of knowledge, improve engine design tools, and enable market-competitive powertrain solutions with potential for best-in-class lifecycle emissions. A special thanks to DOE VTO program managers Mike Weismiller and Gurpreet Singh.

Definitions/Abbreviations

ATDCf	After Top Dead Center Firing
BTDC	before top dead center
CA50	crank angle @ 50% fuel burn
CAD	Crank Angle Degrees
COV	coefficient of variation
DISI	Direct Injected Spark Ignited
ECS	engine control system
EVO	Exhaust Valve Opening

GDI	gasoline direct injection
HR	Spark Plug Heat Range
LHV	Lower Heating Value
MBT	minimum spark advance for maximum brake torque
NIMEP	Net Mean Effective Pressure
ORNL	Oak Ridge National Laboratory

SI	spark ignition
TDCf	Top Dead Center firing